Eurasian Journal of Physics and Functional Materials

2026, 10(3), 302-314

Comparative study of the structural, thermomechanical, and electrical properties of YSZ, ScSZ, and GDC electrolytes for SOFCs

K.Zh. Bekmyrza[1], G.A. Bakalbayeva[1], A.M. Kabyshev[1], N.K. Aidarbekov[1,*], A.A. Baratova[1], M.M. Kubenova[1], M.V. Simakin[2], U. Kokayev[3]

[1]Institute of Physical and Technical Sciences of L.N. Gumilyov Eurasian National University, Astana, Kazakhstan

[2]Sh. Ualikhanov Kokshetau University, Kokshetau, Kazakhstan

[3]L.N. Gumilyov Eurasian National University, Faculty of Transport and Energy Astana, Kazakhstan

E-mail: aidarbekov_nk_1@enu.kz

DOI: **10.32523/ejpfm.2026100309**
Received: 24.09.2026 - after revision

Solid oxide fuel cells require electrolyte materials that combine high oxide-ion conductivity with suitable sintering behavior, thermomechanical compatibility, and structural stability. This study presents a comparative investigation of the structural, thermomechanical, and electrical properties of nanosized yttria-stabilized zirconia (YSZ), scandia-stabilized zirconia (ScSZ), and gadolinium-doped ceria (GDC) powders synthesized by laser evaporation under consistent processing conditions. Phase composition, specific surface area, and particle morphology were characterized by X-ray diffraction, nitrogen adsorption, and transmission electron microscopy. Sintering behavior and linear thermal expansion were investigated by dilatometry, while electrical conductivity was measured using a four-probe direct-current method. All three compositions formed single-phase cubic fluorite-type solid solutions. The average particle sizes were 15.5 nm for YSZ, 10.8 nm for ScSZ, and 24.2 nm for GDC. YSZ exhibited the highest onset temperature of shrinkage but the most intensive subsequent densification, whereas GDC began to shrink at a lower temperature and densified more gradually; ScSZ showed intermediate behavior. The coefficients of thermal expansion were 11.0×10^{-6}, 11.3×10^{-6}, and 12.7×10^{-6} K^{-1} for YSZ, ScSZ, and GDC, respectively. At 800 °C, the electrical conductivity reached approximately 0.04, 0.11, and 0.09 S cm^{-1}, respectively. Comparison with a lanthanum strontium manganite/yttria-stabilized zirconia cathode composite indicated favorable shrinkage matching for ScSZ under the investigated co-sintering conditions. The results demonstrate that electrolyte selection should simultaneously consider electrical conductivity, densification behavior, and thermomechanical compatibility, with ScSZ showing a particularly favorable balance of these properties under the investigated conditions.

Keywords: solid oxide fuel cell; electrolyte nanopowders; YSZ; ScSZ; GDC; electrical conductivity

Introduction

In recent decades, hydrogen has attracted increasing attention as a promising energy carrier that can be produced using renewable energy sources and can contribute to reducing greenhouse gas emissions associated with the use of fossil fuels [1]. Its major advantages include the diversity of available production pathways, the possibility of integration with renewable energy systems, and environmentally benign end use, particularly in fuel cells, where water is the primary reaction product [1].

Solid oxide fuel cells (SOFCs) are electrochemical energy-conversion devices that directly convert the chemical energy of a fuel into electrical energy and heat. Their high conversion efficiency, fuel flexibility, and potential for combined heat and power generation make SOFCs attractive for stationary, distributed, and auxiliary power applications. Nevertheless, the relatively high operating temperatures of conventional SOFCs impose stringent requirements on the chemical, structural, and thermomechanical stability of their functional components and accelerate degradation processes. Consequently, considerable research efforts are currently focused on reducing the operating temperature while retaining sufficiently high electrochemical performance and long-term durability [2–6].

The electrolyte is one of the key functional components of an SOFC because it must combine high oxide-ion conductivity with negligible electronic conductivity, gas tightness, chemical stability, and thermomechanical compatibility with adjacent electrode layers. As the operating temperature decreases, the ohmic contribution of the electrolyte becomes increasingly important, making electrolyte composition, thickness, density, grain structure, and grain-boundary characteristics critical parameters for cell performance [3, 4, 6, 7]. Among fluorite-type oxide-ion conductors, yttria-stabilized zirconia (YSZ), Scandia-stabilized zirconia (ScSZ), and gadolinium-doped ceria (GDC) remain among the most extensively investigated electrolyte systems for high- and intermediate-temperature SOFCs.

YSZ is the most established electrolyte for conventional SOFCs due to its high chemical stability, mechanical reliability, and predominantly ionic conductivity over a wide range of oxygen partial pressures. Its main limitation is the decrease in ionic conductivity with decreasing temperature, which results in increased ohmic losses in the intermediate-temperature range [6, 7]. In addition, fabrication of dense YSZ electrolyte layers generally requires relatively high sintering temperatures, although advanced processing strategies can substantially improve densification at reduced temperatures [8]. Nanostructured YSZ powders therefore remain of considerable interest because their high surface area can enhance sintering activity and enable improved control over the resulting ceramic microstructure [8, 9].

ScSZ is particularly attractive because appropriately scandia-stabilized zirconia can exhibit substantially higher oxide-ion conductivity than conventional YSZ. However, its application is complicated by phase-stability issues and changes in conductivity associated with transformations between highly conductive cubic and less conductive rhombohedral structures [10–12]. Recent studies have consequently focused on compositional modification and sintering additives to

improve both the phase stability and densification behavior of ScSZ. For example, co-doping and the introduction of sintering aids have been shown to reduce the densification temperature while maintaining high conductivity and improved long-term stability [10].

GDC represents another important class of fluorite-type electrolytes and is characterized by comparatively high oxide-ion conductivity at intermediate temperatures. Its transport properties and sintering behavior are strongly influenced by dopant concentration, powder characteristics, grain size, and grain-boundary resistance [7, 13, 14]. However, under reducing conditions, partial reduction of Ce^{4+} to Ce^{3+} may introduce an electronic contribution to the total conductivity, potentially decreasing the ionic transference number when GDC is used as a single electrolyte layer. Recent approaches therefore include multilayer GDC/YSZ architectures designed to combine the high ionic conductivity of GDC with the electronic-blocking and chemical-stability advantages of YSZ [15].

A direct comparison of electrolyte materials based solely on conductivity is insufficient for selecting materials for practical SOFC fabrication. Sintering onset temperature, densification rate, total shrinkage, coefficient of thermal expansion (CTE), and compatibility with adjacent functional layers are equally important. Zhang et al. [7] demonstrated substantial differences in the conductivity of commercially available YSZ, ScSZ, and GDC and emphasized the role of powder processing and microstructure. Thermal-expansion measurements have likewise shown that stabilized zirconia and doped-ceria electrolytes exhibit material-dependent thermomechanical behavior relevant to the development of stresses during cell fabrication and operation [16]. Studies of YSZ and GDC densification further demonstrate that powder characteristics and processing routes can markedly affect the temperatures required to obtain highly dense electrolyte ceramics [8, 13].

These considerations become particularly important during co-sintering of multilayer SOFC structures. Differences in the onset and rate of shrinkage between the electrolyte and electrode layers may generate differential stresses, warping, delamination, or cracking. LSM and LSM:YSZ composites are well-established SOFC cathode materials and therefore provide a useful model system for evaluating cathode–electrolyte compatibility [17, 18]. Recent in-situ investigations of LSM:YSZ densification have demonstrated the complex evolution of the composite microstructure during sintering, emphasizing the importance of matching the thermal processing behavior of electrode and electrolyte layers [18].

Nanopowders produced by laser evaporation provide a useful platform for such comparative investigations because they can exhibit small particle sizes and relatively weak agglomeration. Laser-derived YSZ and GDC nanopowders have previously been employed for the preparation of dense SOFC electrolytes and multilayer ceramic structures [19]. Nanostructured GDC has also continued to attract interest for improving electrode/electrolyte interfaces and electrochemical performance in microtubular SOFCs [20]. These studies indicate that control of nanopowder characteristics can provide an effective means of tailoring both sintering behavior and functional properties.

In the present work, a systematic comparative investigation of $Zr_{0.84}Y_{0.16}O_{2-\delta}$

(YSZ), $Zr_{0.81}Sc_{0.19}O_{2-\delta}$ (ScSZ), and $Ce_{0.73}Gd_{0.27}O_{2-\delta}$ (GDC) electrolyte materials prepared from laser-evaporated nanopowders was carried out. The materials were comparatively characterized in terms of phase composition, specific surface area, particle morphology, sintering behavior, thermal expansion, and electrical conductivity. Particular attention was paid to establishing relationships between the structural and morphological characteristics of the nanopowders and the thermomechanical and electrical properties of the resulting ceramic electrolytes. In addition, the shrinkage behavior of the zirconia-based electrolytes was compared with that of LSM and an LSM:YSZ composite in order to assess their compatibility during co-sintering. The aim of this study was to provide an integrated comparison of the structure-processing-property relationships of YSZ, ScSZ, and GDC and to evaluate their advantages and limitations for application as SOFC electrolyte materials.

Materials and methods

Preparation of electrolyte nanopowders

Nanosized powders of the electrolyte materials $Zr_{0.84}Y_{0.16}O_{2-\delta}$ (YSZ), $Zr_{0.81}Sc_{0.19}O_{2-\delta}$ (ScSZ), and $Ce_{0.73}Gd_{0.27}O_{2-\delta}$ (GDC) were synthesized by the laser evaporation method. The target materials used for nanopowder production were prepared from YSZ powder obtained by solid-state synthesis, a mechanical mixture of Sc_2O_3 and ZrO_2 powders with a mass ratio of 0.114, and a mechanical mixture of Gd_2O_3 and CeO_2 powders with a mass ratio of 0.381. The targets were compacted using an ARMADA TG1220MA uniaxial hydraulic press (20-ton capacity; ARMADA, Russia) and subsequently sintered at 1300 °C for 1 h. The resulting targets were disk-shaped, with a diameter of approximately 60 mm and a thickness of approximately 20 mm. Nanopowder synthesis was carried out using an LK-1 ytterbium fiber laser equipped with a Riedel PC-41.02-KE-S chiller and an Optoskand d25 f60/200 optical head. The laser was operated in a modulated (pulsed-periodic) mode at a repetition frequency of 5 kHz and a pulse duration of 100 μs. The laser power was 450 W, and the emission wavelength was 1.07 μm. Nanopowders were synthesized in an air atmosphere at atmospheric pressure.

Following synthesis, the obtained powders were annealed at 1000 °C for 4 h to induce controlled, moderate particle coarsening. All subsequent investigations of the thermal properties and electrical conductivity, as well as the preparation of specimens for evaluating electrode characteristics, were performed using the annealed powders.

Powder characterization

The phase composition of the investigated materials was determined by X-ray diffraction (XRD) using a D8 DISCOVER diffractometer with Cu K$\alpha_{1,2}$ radiation ($\lambda = 1.542$ Å) and a graphite monochromator positioned in the diffracted beam. The diffraction data were analyzed using TOPAS 3 software employing the

Rietveld refinement method for the determination of structural parameters. The average crystallite size was estimated using the Scherrer equation with a shape factor, K, of 0.89.

The specific surface area of the powders was determined by low-temperature nitrogen adsorption using the Brunauer-Emmett-Teller (BET) method on an automated TriStar 3000 surface area analyzer. Assuming a spherical particle morphology, the average particle diameter was calculated according to the following equation:

$$d_{BET} = \frac{6}{\rho_{th} S_{BET}} \tag{1}$$

where d_{BET} is the average particle diameter, S_{BET} is the specific surface area of the powder, and ρ_{th} is the theoretical density of the corresponding material.

The morphology of the synthesized powders was examined by electron microscopy using a JEOL JEM-2100 transmission electron microscope (TEM) and LEO 982 and JEOL JSM-6390LA scanning electron microscopes (SEM).

Sintering behavior and thermal expansion

The sintering behavior of the materials was investigated using disk-shaped specimens with a diameter of 8 mm and a thickness of approximately 3 mm. The specimens were uniaxially compacted to a relative density of approximately 50–70% of the theoretical density using an ARMADA TG1220MA hydraulic press (20-ton capacity; ARMADA, Russia).

The linear thermal expansion measurements were performed using rectangular bar-shaped specimens with dimensions of approximately $4 \times 4 \times 9.5$ mm. Prior to the measurements, the specimens were sintered to densities close to their theoretical values.

The thermomechanical properties of the investigated materials were studied using a NETZSCH DIL 402C dilatometer. The sintering behavior of the compacted powder specimens was investigated in air over the temperature range of 20–1500 °C. The linear thermal expansion of the sintered specimens was measured during heating from room temperature to 1200 °C in static air. All measurements were performed at a constant heating rate of 5 °C min^{-1}.

Electrical conductivity measurements

For electrical conductivity measurements, the investigated powders were uniaxially compacted into rectangular bar-shaped specimens with typical dimensions of approximately $3 \times 2 \times 30$ mm. The compacted specimens were subsequently sintered in air. The sintering temperatures were selected based on the dilatometric data obtained from the shrinkage measurements. The electrolyte specimens were sintered at 1400 °C for 10 h.

After sintering, platinum-wire probes with a diameter of 0.2 mm were attached to the specimens according to the four-probe configuration shown in Figure 6. To ensure reliable electrical contact between the platinum probes and the specimen

surface, platinum paste was applied at the contact points and subsequently fired at 1000 °C for 1 h.

The electrical conductivity of the investigated materials was measured using a four-probe direct-current (DC) method. Measurements of the electrolyte materials were carried out in static air. The electrical conductivity of the electrolyte materials was measured using a P-40X instrument, whereas the electrical properties of the cathode and anode materials were measured using an LCR-76100 precision LCR meter.

Results and discussion

The X-ray diffraction (XRD) patterns of the synthesized YSZ, ScSZ, and GDC powders are shown in Figure 1. All investigated compositions exhibit well-defined diffraction reflections characteristic of a cubic fluorite-type structure with the *Fm*–3*m* space group. No additional reflections attributable to secondary or impurity phases were detected within the sensitivity of the XRD technique, indicating the formation of single-phase solid solutions.

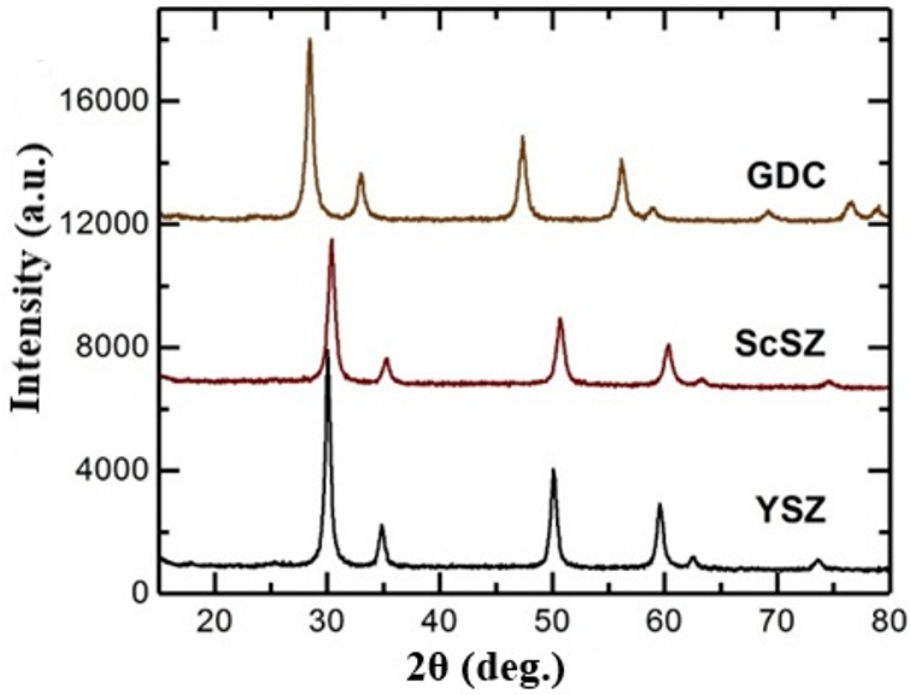

Figure 1. XRD patterns of the synthesized YSZ, ScSZ, and GDC electrolyte powders.

The positions of the diffraction peaks vary depending on the electrolyte composition. The characteristic reflections of GDC are shifted toward lower 2θ values compared with those of YSZ and ScSZ, which is associated with the larger lattice parameter of GDC. In contrast, ScSZ exhibits the highest 2θ positions of the corresponding reflections, consistent with its smaller lattice parameter. These observations are in good agreement with the lattice parameters obtained from the Rietveld refinement and confirm the compositional dependence of the unit-cell dimensions of the investigated fluorite-type solid solutions.

Table 1.
Physicochemical characteristics of the synthesized electrolyte powders

Powder	S_{BET}, $m^2/g^{-}1$	d_{BET}, nm	Space group	Lattice parameter, Å	ρ_{XRD}, g cm^{-3}
YSZ	65.3	15.5	Fm-3m	$a = 5.143$	5.94
ScSZ	97.4	10.8	Fm-3m	$a = 5.087$	5.70
GDC	34.2	24.2	Fm-3m	$a = 5.424$	7.25

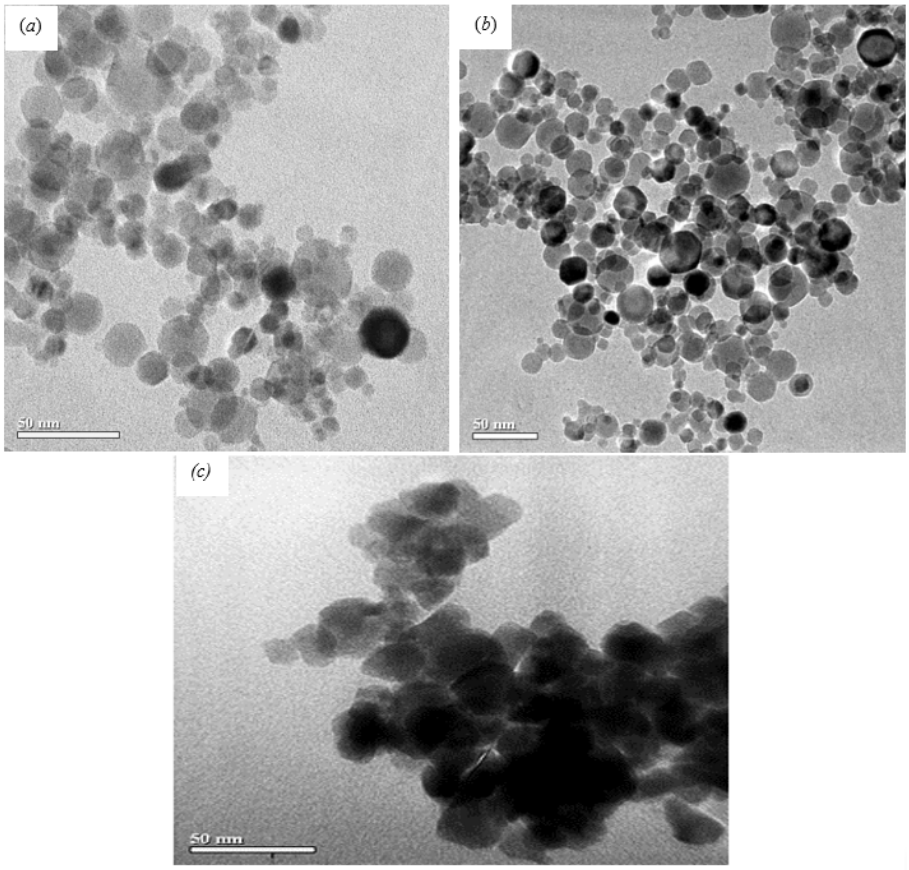

Figure 2. TEM micrographs of the synthesized electrolyte powders: *(a)* YSZ, *(b)* ScSZ, and *(c)* GDC.

The TEM micrographs of the synthesized YSZ, ScSZ, and GDC powders are shown in Figure 2. The YSZ and ScSZ powders consist predominantly of nearly spherical nanoparticles, whereas the GDC particles exhibit a more faceted morphology with rounded edges. A certain degree of particle agglomeration is observed for all compositions, which is characteristic of nanosized oxide powders due to their high specific surface energy. The particle dimensions observed by TEM are generally consistent with the average particle sizes estimated from the BET specific surface area.

As summarized in Table 1, ScSZ exhibits the highest specific surface area and, consequently, the smallest average particle size, whereas GDC has the lowest specific surface area and the largest average particle size. YSZ exhibits intermediate values of both parameters. These results indicate that the specific surface area is inversely correlated with the characteristic particle size of the investigated powders.

All three electrolyte powders crystallize in the cubic fluorite-type structure with the *Fm–3m* space group. The lattice parameter increases in the order ScSZ $<$ YSZ $<$ GDC, which is consistent with the relative positions of the corresponding diffraction peaks in the XRD patterns. The combination of XRD, BET, and TEM results confirms the formation of single-phase nanosized electrolyte powders with composition-dependent structural and morphological characteristics.

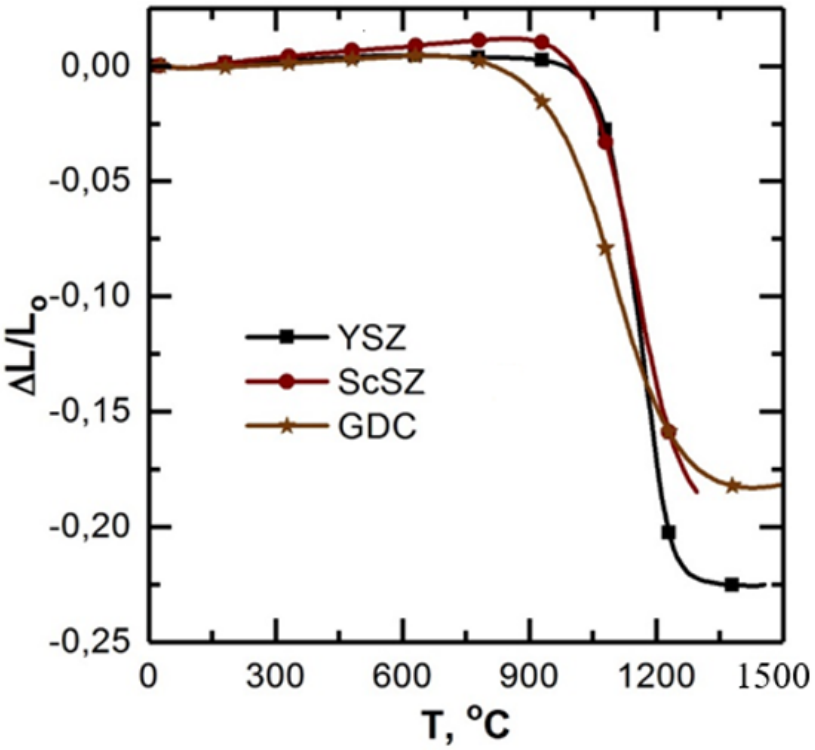

Figure 3. Dilatometric linear shrinkage curves of the YSZ, ScSZ, and GDC electrolyte materials.

Figure 3 shows the dilatometric shrinkage curves of the YSZ, ScSZ, and GDC electrolyte materials. The investigated compositions exhibit pronounced differences in both the onset temperature and the subsequent densification behavior. Although YSZ is characterized by the highest onset temperature of sintering, it also exhibits the most intensive shrinkage at elevated temperatures. This behavior enables the formation of highly densified YSZ ceramics at temperatures below approximately 1300 °C. In contrast, the onset of shrinkage for GDC occurs at a temperature approximately 200 °C lower than that observed for YSZ. However, the subsequent densification proceeds more gradually, indicating a lower shrinkage rate over the investigated temperature range. Consequently, the preparation of highly dense GDC ceramics requires temperatures of approximately 1400 °C or, alternatively, prolonged isothermal holding at lower temperatures.

The sintering behavior of ScSZ is intermediate between those of YSZ and GDC. Its shrinkage begins at a higher temperature than that of GDC, while the rate of densification is lower than that observed for YSZ. At the end of the heating cycle, YSZ exhibits the largest total linear shrinkage, whereas lower final shrinkage values are observed for ScSZ and GDC. These differences indicate a pronounced influence of electrolyte composition on the densification behavior of

the investigated nanopowder-derived ceramics.

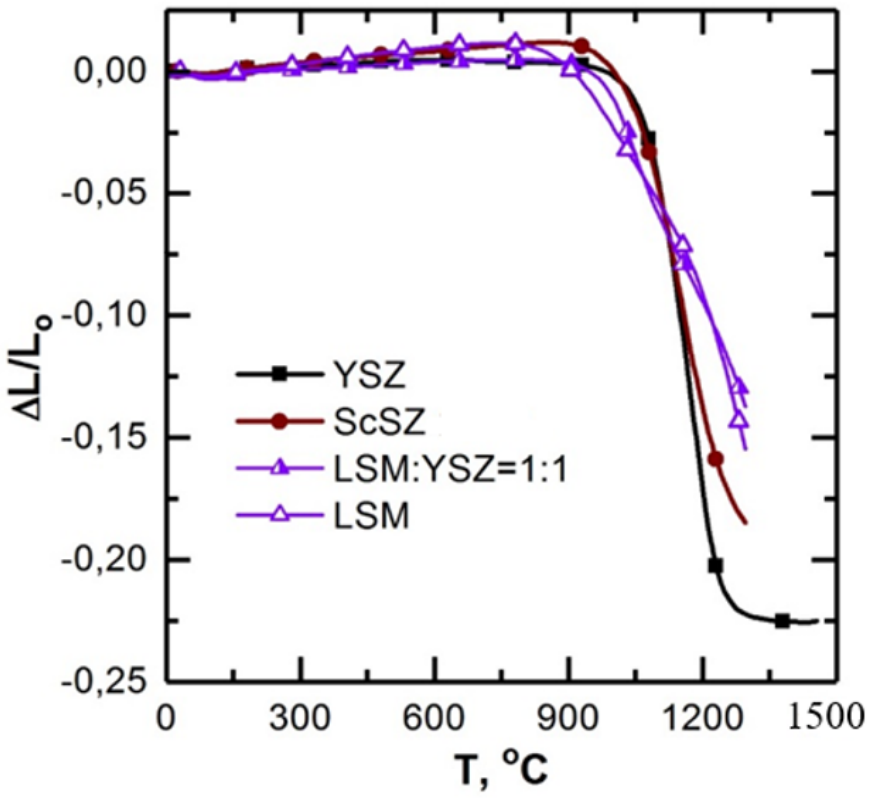

Figure 4. Comparison of the dilatometric linear shrinkage behavior of YSZ and ScSZ electrolytes with LSM and the LSM:YSZ (1:1) cathode composite.

Figure 4 compares the dilatometric shrinkage behavior of pure LSM and the LSM:YSZ (1:1) composite with that of the YSZ and ScSZ electrolyte materials. As can be seen, the onset of shrinkage of pure LSM occurs approximately 200 °C earlier than that of YSZ and ScSZ, indicating a considerable difference in their sintering behavior.

LSM was selected as a representative cathode material because it is a well-established and extensively studied cathode for solid oxide fuel cells. In addition, LSM is commonly used in combination with zirconia-based electrolytes, which makes it suitable for evaluating the compatibility of cathode and electrolyte materials during co-sintering. To improve the electrochemical and thermomechanical compatibility of the cathode with the electrolyte, an LSM:YSZ (1:1) composite was also investigated.

The incorporation of YSZ into LSM shifts the shrinkage behavior of the resulting LSM:YSZ (1:1) composite toward that of the zirconia-based electrolytes, thereby improving the matching of their densification profiles. However, YSZ exhibits a more intensive shrinkage at elevated temperatures and reaches a higher total linear shrinkage than the LSM-based composite.

In contrast, the shrinkage behavior of ScSZ shows closer agreement with that of the LSM:YSZ (1:1) composite over the main densification temperature range. This result indicates that ScSZ may provide more favorable co-sintering compatibility with the LSM-based composite under the investigated thermal

conditions. A closer match between the shrinkage behavior of the cathode and electrolyte layers is important for minimizing differential shrinkage, residual mechanical stresses, cracking, delamination, and other defects that may develop during the co-firing of multilayer SOFC structures.

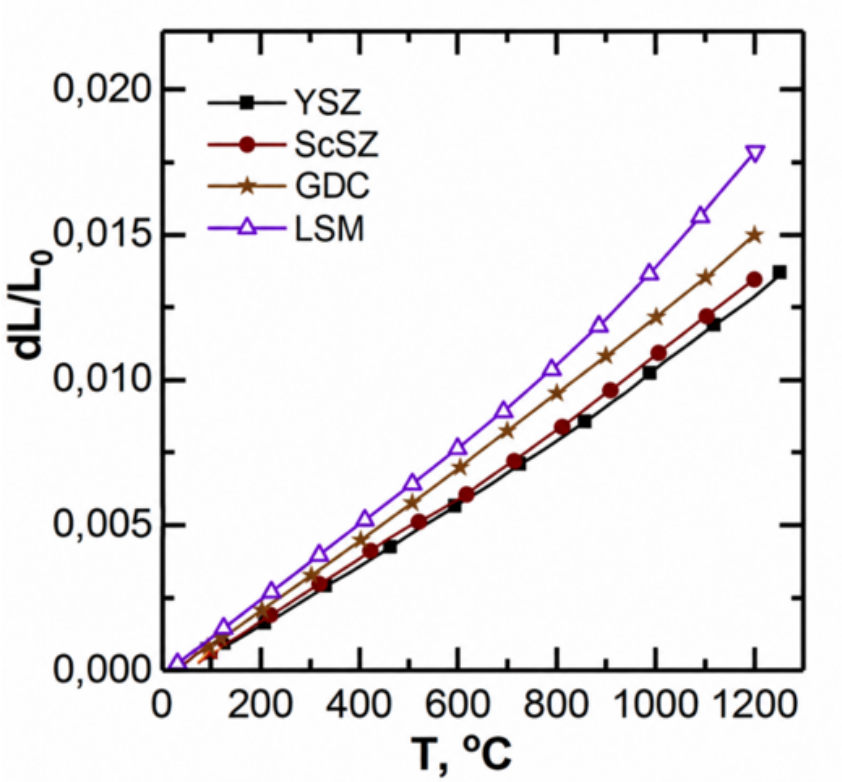

Figure 5. Temperature dependence of the linear thermal expansion of YSZ, ScSZ, GDC, and LSM materials.

Figure 5 presents the results of the linear thermal expansion measurements for the investigated materials. As can be seen, all electrolyte materials exhibit similar coefficients of thermal expansion (CTE), with values ranging from 11.0 to 12.7×10^{-6} K^{-1}.

The calculated CTE values of the investigated electrolyte materials are summarized in Table 2.

Table 2.
CTE of the investigated materials.

Material	Temperature range (ΔT, °C)	CTE (10^{-6} K^{-1})
YSZ	100–1200	11.0
ScSZ	100–1200	11.3
GDC	100–1200	12.7
LSM	100–900	12.9

The temperature dependences of the electrical conductivity of the YSZ, ScSZ, and GDC electrolyte materials are presented in Figure 7. The measured conductivity values are generally consistent with those reported in the literature [21].

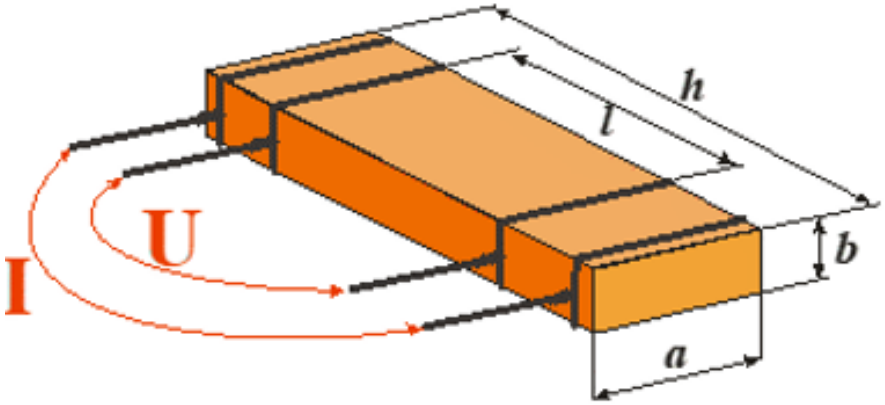

Figure 6. Schematic illustration of the four-probe configuration used for electrical conductivity measurements.

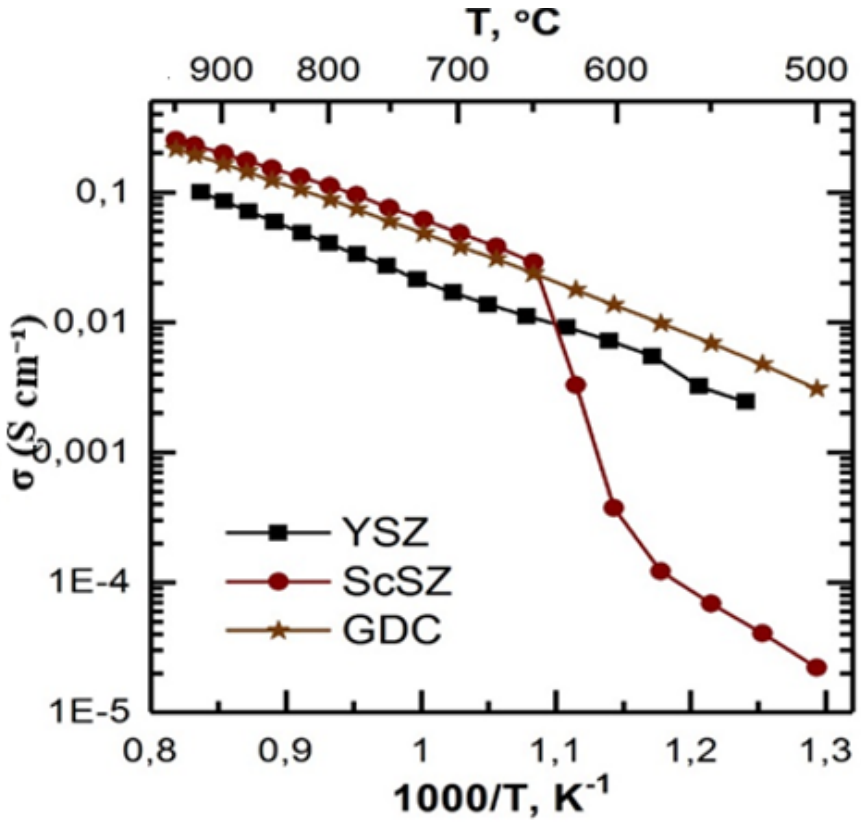

Figure 7. Temperature dependence of the electrical conductivity of YSZ, ScSZ, and GDC electrolyte materials.

At temperatures above approximately 650 °C, ScSZ and GDC exhibit substantially higher electrical conductivity than YSZ. Their conductivity values are approximately 2–2.7 times higher than that of YSZ in the high-temperature region. Among the investigated materials, ScSZ exhibits the highest conductivity, followed by GDC and YSZ.

At 800 °C, the electrical conductivity of ScSZ reaches approximately 0.11 S cm^{-1}, whereas the corresponding values for GDC and YSZ are approximately 0.09 and 0.04 S cm^{-1}, respectively. Thus, both ScSZ and GDC demonstrate a significant conductivity advantage over YSZ at elevated temperatures.

However, below approximately 650 °C, the electrical conductivity of ScSZ decreases markedly. According to previous studies [22, 23], this behavior is associated with structural changes involving the transformation of the cubic phase toward a rhombohedral phase, which adversely affects oxygen-ion transport. Consequently, although ScSZ demonstrates the highest conductivity in the high-temperature range, its conductivity behavior at lower temperatures should also be considered when selecting an electrolyte material for SOFC applications.

Conclusion

A comparative study of the structural, thermomechanical, and electrical properties of YSZ, ScSZ, and GDC electrolytes prepared from laser-evaporated nanopowders was performed. XRD analysis confirmed the formation of single-phase cubic fluorite-type solid solutions with the *Fm*–3*m* space group. The average particle sizes were 15.5 nm for YSZ, 10.8 nm for ScSZ, and 24.2 nm for GDC, with ScSZ exhibiting the highest specific surface area and the smallest particle size.

Dilatometric measurements revealed significant differences in sintering behavior. YSZ exhibited the highest onset temperature of shrinkage but the most intensive subsequent densification, whereas GDC started to shrink at a lower temperature and densified more gradually; ScSZ showed intermediate behavior. The shrinkage profile of ScSZ also showed comparatively good agreement with that of the LSM:YSZ (1:1) cathode composite, indicating favorable co-sintering compatibility under the investigated conditions. The coefficients of thermal expansion were 11.0×10^{-6} K^{-1} for YSZ, 11.3×10^{-6} K^{-1} for ScSZ, and 12.7×10^{-6} K^{-1} for GDC.

At 800 °C, the electrical conductivity values were approximately 0.04 S cm^{-1} for YSZ, 0.11 S cm^{-1} for ScSZ, and 0.09 S cm^{-1} for GDC. Thus, ScSZ exhibited the highest conductivity among the investigated electrolytes and, together with its favorable thermomechanical compatibility, demonstrated a promising combination of properties for SOFC applications. Overall, the results show that electrolyte selection should consider not only electrical conductivity but also sintering behavior, thermal expansion, and compatibility with adjacent functional layers.

The overall results confirm that the optimal selection of an electrolyte material for solid oxide fuel cells is determined by a balance between ionic conductivity, phase stability, sintering behavior, and thermomechanical compatibility with adjacent functional layers. In this respect, ScSZ is of particular interest for high-conductivity electrolyte layers, whereas YSZ and GDC retain significant potential depending on the operating temperature range and the specific cell architecture.

Acknowledgments

This work was supported by the Science Committee of the Ministry of Science and Higher Education of the Republic of Kazakhstan (Grant No. AP26104931).

References

[1] K.Zh. Bekmyrza et al., Int. J. Low-Carbon Technol. **20** (2025) 1554–1570. [*CrossRef*]
[2] P. Feng et al., eScience **6**(2) (2026) 100460. [*CrossRef*]
[3] D. Sikstrom, V. Thangadurai, Ionics **32** (2026) 5–30. [*CrossRef*]
[4] J. Li et al., Mater. Adv. **6**(1) (2025) 39–83. [*CrossRef*]
[5] K.A. Kuterbekov et al., Int. J. Low-Carbon Technol. **20** (2025) 353–367. [*CrossRef*]
[6] P. Vinchhi et al., Inorg. Chem. Commun. **152** (2023) 110724. [*CrossRef*]
[7] J. Zhang et al., Solid State Ionics **344** (2020) 115138. [*CrossRef*]
[8] Q. Lai et al., Ceram. Int. **49**(9) (2023) 14744–14749. [*CrossRef*]
[9] A. Hatipogullari et al., Ceram. Int. **50**(5) (2024) 7723–7736. [*CrossRef*]
[10] Z.-M. Zhang et al., Int. J. Hydrogen Energy **139** (2025) 425–434. [*CrossRef*]
[11] S. Kazlauskas et al., Solid State Ionics **310** (2017) 143–147. [*CrossRef*]
[12] M. Okamoto et al., Solid State Ionics **176**(7–8) (2005) 675–680. [*CrossRef*]
[13] M. Murutoglu et al., Int. J. Hydrogen Energy **47**(45) (2022) 19772–19779. [*CrossRef*]
[14] N. Ghaemi et al., Ceram. Int. **50**(21) (2024) 41780–41791. [*CrossRef*]
[15] H. Dang et al., Fuel **407** (2026) 137482. [*CrossRef*]
[16] P. Gao et al., Solid State Ionics **300** (2017) 1–9. [*CrossRef*]
[17] J. Nielsen, J. Hjelm, Electrochim. Acta **115** (2014) 31–45. [*CrossRef*]
[18] M. Carda et al., Electrochim. Acta **482** (2024) 143979. [*CrossRef*]
[19] V.V. Ivanov et al., J. Power Sources **159**(1) (2006) 605–612. [*CrossRef*]
[20] M.J. López-Robledo et al., Ceram. Int. **41** (2015) 7651–7660. [*CrossRef*]
[21] J.W. Fergus, J. Power Sources **162**(1) (2006) 30–40. [*CrossRef*]
[22] O. Yamamoto et al., Solid State Ionics **79** (1995) 137–142. [*CrossRef*]
[23] S.P.S. Badwal et al., Solid State Ionics **136–137** (2000) 91–99. [*CrossRef*]